IEEE Access
Multidisciplinary | Rapid Review | Open Access Journal

Received 16 May 2023, accepted 25 June 2023, date of publication 4 July 2023, date of current version 12 July 2023.

Digital Object Identifier 10.1109/ACCESS.2023.3292275

RESEARCH ARTICLE

Underwater Image Enhancement Based on Optimal Contrast and Attenuation Difference

TENGHUI WANG[1,2], LILI WANG[1,3], EN ZHANG[1,3], YAN MA[2], YAPENG WANG[2], (Member, IEEE), HAIJUN XIE[1,3], AND MINGCHAO ZHU[1,3]

[1]Beijing Institute of Technology, Zhuhai 519088, China
[2]Faculty of Applied Sciences, Macao Polytechnic University, Macau 999078, China
[3]Beijing Institute of Technology, Beijing 100081, China

Corresponding author: Lili Wang (w18676137171@163.com)

This work was supported in part by the Key Platform and Scientific Research Project for General Universities, Guangdong, in 2022, under Grant 2022ZDZX4061; in part by the Science and Technology Program of Social Development, Zhuhai, in 2022, under Grant 2220004000195; in part by the Featured Innovation Projects of Guangdong of Education, Guangdong, in 2022, under Grant 2022KTSCX197; in part by the Guangdong Provincial Key Laboratory of Interdisciplinary Research and Application for Data Science, Beijing Normal University & Hong Kong Baptist University (BNU-HKBU) United International College, under Project 2022B1212010006; and in part by the Guangdong Higher Education Upgrading Plan (2021–2025) with United International College (UIC) under Grant R0400001-22 and Grant R201902.

ABSTRACT The quality of underwater images is often marred by noticeable color casts and blurring, resulting from complex phenomena such as differential light attenuation based on wavelength, veiling light scattering, and light scattering by plankton and suspended particles in water. In this paper, we propose an effective underwater image enhancement method called Optimal Contrast and Attenuation Difference (OCAD) to tackle these issues. The OCAD method employs a two-step approach. First, it estimates a coarse transmission map by optimizing contrast and minimizing information loss during image mapping. This transmission map is then refined using a combination of dark channel prior and guided filter refining techniques to improve its accuracy. Second, OCAD estimates the veiling light by considering the differential attenuation of red, green, and blue light underwater. This estimated veiling light is utilized to partially mitigate the color cast caused by the attenuation effect, while also addressing the blurring based on an imaging model. To further enhance the image quality, we introduce the Gray World approach to correct the color and obtain a deblurred and color-corrected underwater image. To evaluate the performance of our proposed method, extensive experiments are conducted on well-established underwater image datasets, including the EUVP, UIEB, and RUIE datasets. Comparative analysis against state-of-the-art and classical underwater image enhancement methods reveals that our OCAD algorithm significantly enhances underwater images and outperforms other methods in terms of image quality improvement.

INDEX TERMS Underwater images enhancement, underwater deblur, underwater color correction.

I. INTRODUCTION

Marine resources are abundant, and underwater imaging technologies play a crucial role in providing clear images and video information of the underwater environment, making them indispensable for the exploration and exploitation of marine resources. However, the challenging underwater environment, influenced by factors such as light attenuation and scattering effects, often results in poor-quality of collected underwater images. Therefore, there is a pressing need for advanced underwater image enhancement technologies to effectively address the issues of low-quality underwater images and improve their visual quality [1].

Different from the atmospheric environment, the attenuation coefficients of different wavelengths of light in water are different, resulting in color distortion, contrast, and brightness decrease in underwater images. As shown in Figure 1, red light with a long wavelength is absorbed preferentially in clear sea water and travels the shortest distance, followed by orange, yellow, green, and blue light. Therefore, Marine

The associate editor coordinating the review of this manuscript and approving it for publication was Akansha Singh.

This work is licensed under a Creative Commons Attribution-NonCommercial-NoDerivatives 4.0 License.
For more information, see https://creativecommons.org/licenses/by-nc-nd/4.0/

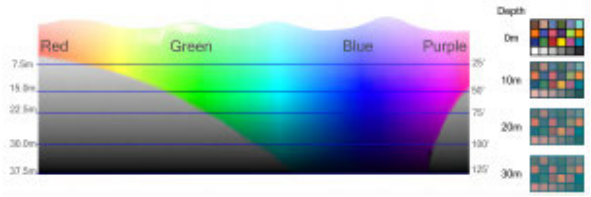

FIGURE 1. The selective fading of light under water.

FIGURE 2. The hue of underwater images tends to be close to green and blue.

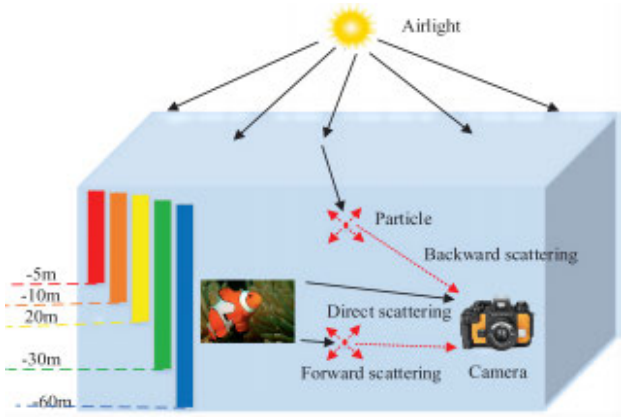

FIGURE 3. Schematic diagram of underwater imaging.

water bodies are often blue-green [2]. We refer to the effect that different wavelengths of light are absorbed differently by water as the attenuation effect. Due to the attenuation effect, our underwater images tend to have a blue or green hue. As shown in Figure 2, the blue hues are those taken in the deep sea, and the green hues are those taken relatively close to the surface.

A schematic diagram of the camera taking images underwater with the lighting conditions as an illuminated light source is shown in Figure 3. Suspended particles or plankton in the water scatter the ambient background light and the light propagating from the target scene to the camera. The imaging sensors eventually capture these lights, resulting in blurred details and making the image shrouded in a dense fog [3]. In near-surface waters and rivers where water moves faster, sediment and other suspended particles or plankton concentration are generally much higher than in calm, deep waters. The closer to the surface, the higher the water velocity and the higher the concentration of contaminants in the water.

The image shown in figure 4 was taken at our aquaculture farm, where we placed a green target near the shore to take the picture, with only natural light as illumination. The high concentration of impurities in the water from active fish,

FIGURE 4. Pictures taken on the bank of a fish pond.

including the excretion of fish waste and the dissolution of excess fish food, made image sensors almost impossible to capture a clear image. Only the object's outline can be roughly seen. This shows that when the concentration of impurities in the water is too high, the scattering of light by the impurities greatly blurs the underwater image. We refer to these effects as the scattering effect.

The camera acquires imaging information from three components, as shown in figure 3:

$$E = E_d + E_f + E_b. \tag{1}$$

where E indicates the information captured by the camera and processed by the camera to provide us with the image information.E_d denotes the information transmitted directly from the target scene to the camera, which contains real information about the target scene and is the signal we need. E_f refers to the part of the light propagation from the target scene to the camera where the light is scattered by suspended particles or plankton on its way to producing stray light and is picked up by the camera, called the forward scattering. E_b indicates the fraction of suspended particles in the water that scatter the illumination light to produce stray light and are picked up by the camera, called the backscatter.

Current underwater imaging sensors cannot capture images underwater without the illumination source. Generally, the maximum distance the illumination source can reach is the maximum distance from which the device can capture the image. In general, the distance between the target scene and the camera in underwater imaging is short due to the limited illumination range of the light source. In our experiments, using a single LED light as the underwater light source, we found that the camera could hardly capture images underwater at a distance greater than 10 meters. Therefore, our experiments limit the distance between the camera and the target scene to 5 meters. We also checked the literature and found that most target scenes for underwater photography are set at a relatively short distance from the camera. Because of the shorter distance, shortening the propagation path reduces the amount of suspended particles or plankton appearing in the propagation path. In other words, very few suspended particles or plankton are expected to be in the path from the target to the camera, which is negligible. After a long period of research, it has been found that forward scattering has little effect on the image of underwater photographs. Therefore, most studies have ignored E_f in Equation (1) [4].

With the development of computer vision, after a long period of analysis, researchers usually accept the equation linking underwater imaging model with image pixel [5] as shown in Equation (2).

$$I^C(x,y) = J^C(x,y)t^C(x,y) + A^C\left(1 - t^C(x,y)\right). \quad (2)$$

where $C \in \{R, G, B\}$, I^C (x, y) is the C channel of the underwater image captured by the camera, A^C is veiling light. J^C (x, y) is the C channel of the real view of the target scene, and J^C (x, y) is also the target image we restored. $t^C(x,y) = e^{-\beta^C r}$ is the transmission map, which represents the transmission of light from the target scene to the camera and takes the values [0,1], And r represents the distance between the camera and target scene. In the same propagation medium, we consider the attenuation coefficient of the light and the ambient background light as constants, so β^C is a constant. The model of Equation (2) is widely used in underwater imaging [6], [7], [8], [9], [10] gives a profound and detailed analysis related attenuation coefficient. Section III presents our OCAD method based on this model in detail.

Our Contribution to this work is as follows:

1. In our OCAD method, we proposed estimating the transmission map based on the optimal contrast and the minimum information loss in mapping between ideal and degraded underwater images. The method can effectively improve the estimation of the transmission map of underwater images.

2. Our OCAD method proposes an ambient background light estimation method based on the difference in the attenuation of red, green, and blue light underwater, allowing partial color correction of the underwater image while deblurring it based on the imaging model.

3. We combine the physical model based underwater image enhancement method and the Gray World algorithm to provide a new deblur and color correction method for underwater image enhancement. The test result shows that our method is significantly more quantitatively and qualitatively effective than existing underwater image enhancement methods.

II. RELATED WORK

Some researchers use optical hardware technology and sonar technology to acquire information underwater, e.g., polarization imaging, range-gated imaging [11], [12], [13], [14], [15], multi-beam sonar [16]. Our work is mainly based on image processing algorithms [14], [17] to enhance low-quality underwater images, so this paper mainly presents the work related to image algorithms. Since the physical model of fog imaging is like underwater imaging, some dehazing algorithms have been extended to deblurring underwater images [18], [19].

After extensive data analysis, He [20] discovered common differences between fog maps and general images and proposed the classical prior theory of the dark channel. The dark channel, a prior theory based on data analysis from many fog-free outdoor images, suggests that the pixel values in at least one-color channel in fog-free images are tiny in most areas, excluding the sky, in RGB color space. Expressed as an equation, this is shown in Equation (3).

$$J^{dark}(x,y) = \min_{c\in\{r,g,b\}}\left(\min_{(x,y)\in\Omega} J^c(x,y)\right) \approx 0. \quad (3)$$

This equation indicates that the minimum value of the image I in one of the channels of RGB at the position of the region (x, y) tends to zero, which is approximated as zero. The dark channel, a prior theory proposed by He, suggests a new method for calculating the transmission rate image, shown in Equation (4).

$$t(x,y) = 1 - \min_{c\in\{r,g,b\}}\left(\min_{(x,y)\in\Omega}\frac{I^c(x,y)}{A^c}\right) \quad (4)$$

After the Dark Channel Prior theory, He [20] proposed Soft-Matching, and Guided Filtering [21] to refine the transmission map. Because the transmission map is calculated based on the image block and the region will make the defogging result uneven, some regions in the image appear halo that covers the details.

Han [22] introduced the principles of various underwater image enhancement tasks and compared their effects. They divided underwater image enhancement methods into two categories, underwater image deblurring and underwater image color correction. Our research divided the underwater image enhancement methods into pixel-based and physical model-based underwater imaging. Pixel-based methods include the relative global histogram stretching (**RGHS**) method proposed by Huang [23]. This method processes the image in RGB and CIE-Lab color space and stretches the histogram of the image to enhance the quality of the image.

The following methods are all based on the physical model of underwater imaging. The difference is whether the deep learning [24] method is introduced. Based on the physical model of underwater images, Wei [25] proposed Underwater Light Appreciation Prior (**ULAP**) to estimate the parameters of the model, ambient background light, and transmission.

Considering the attenuation coefficient of different wavelengths of light in different water types, Berman [26] established the attenuation ratio model of blue-red and blue-green light and converted the underwater image deblurring problem into a single image defogging problem. Since the water quality type of the target scene is unknown, the paper obtains some restoration images with different effects based on the attenuation coefficient of light of all known water quality types. These results are automatically filtered according to the color distribution, and the best results are selected simultaneously as color correction. Li [27] proposed an underwater image enhancement convolutional neural network(CNN) model based on underwater scenes prior, called UWCNN. This work first synthesizes underwater image degradation datasets by combining an underwater imaging physical model with the optical properties of underwater scenes. The effect of this method mainly depends on how similar the synthetic degradation dataset is

to the image degradation effect in the underwater environment. Liu [28] proposed an object-guided twin adversarial contrastive learning-based underwater enhancement method. Ma and Oh [29] decomposed the underwater and corresponding ground truth images into different frequency bands and then trained two sub-nets by supervised learning. However, the synthetic and flawed datasets also limit the removing water ability of this method. This method is similar to our previous work [30], we decomposed underwater images into a base layer, and a detail layer via filters, but our previous work is the unphysical model method. Islam [31] presented a conditional generative adversarial network-based model, named **FUnIE**, for real-time underwater image enhancement and created EUVP (Enhancing Underwater Visual Perception) dataset, We experimented on this dataset. Chen [32] proposed an underwater image enhancement algorithm based on the underwater image physical model and the depth learning method. This method can effectively eliminate the influence of the underwater environment on the imaging, enrich the color, and enhance the underwater image details. In this article, we call this method **IFM**. In Section IV, we compared with **RGHS**, **ULAP**, **FUnIE**, **IFM** methods.

We planned to introduce the color correction parameter into the underwater imaging model, along with the idea that underwater image enhancement tasks can divide underwater image deblurring and underwater image color correction. It is only possible to completely reconstruct the underwater target scene in the land environment with the effect of water; there is significant uncertainty in the relevant data, dramatically impacting the results based on the neural network method. So, we proposed a new underwater image enhancement based on an underwater imaging model without deep learning.

III. OPTIMAL CONTRAST AND ATTENUATION DIFFERENCE (OCAD)

In this study, we proposed OCAD for optimal estimation of the model parameters, veiling light, and transmission map based on the underwater imaging model.

Firstly, we estimate the coarse transmission map based on the optimal contrast and minimum information loss during image mapping between the original underwater image and the ideal underwater image. Then, we optimize the coarse transmission map by considering the dark channel prior estimation of the transmission map. The specific step is to take the larger value of the corresponding position. Then the optimal transmission map is refined by the Guided Filter.

Secondly, we estimate the veiling light based on the different attenuation of underwater red, green, and blue light. This veiling light can partially eliminate the color deviation of the underwater image caused by the attenuation effect while deblurring based on the imaging model. As shown in figure 5, the red dot in the red box in the second figure on the left is the pixel that can express the ambient background light of the environment found by our OCAD method.

Thirdly, we introduce the Gray World to correct the image color further and obtain a deblurred and color-corrected underwater image.

A. TRANSMISSION MAP ESTIMATION

Through many experiments, we found that the contrast of underwater images is lower than that of ground truth images, especially the contrast of areas seriously affected by scattering in the image is lower than that of other parts of the image.

We used the mean square deviation to reflect the contrast of the image. The mean square deviation reflects the fluctuation of the data from the mean value. The larger the mean square deviation of the image, the more significant the difference between the pixels of the image and the more excellent contrast of the image. Figure 6 shows the *Con* of the ground truth image, the corresponding blurred underwater image, and the *Con* value that reflects their contrast. The *Con* value of ground truth underwater images is greater than that of corresponding blurred underwater images.

$$\mathrm{Con} = \sum_{\mathrm{C}\in\{\mathrm{R,G,B}\}} \sum_{(\mathrm{x,y})} \frac{\left(J^{\mathrm{C}}(\mathrm{x,y}) - \overline{J^{\mathrm{C}}(\mathrm{x,y})}\right)^2}{\mathrm{N}} \tag{5}$$

where $\overline{J^C(x,y)}$ represents the average value of the ideal image's C channel, $J^C(x,y)$ represents the value of the pixel at (x,y) in C channel, N represents the total number of pixels. Compared with the degraded underwater image affected by the scattering effect and attenuation effect, the *Con* of the ideal image reflecting the real information of the target scene should be more outstanding.

From Equation (2), we can obtain:

$$\begin{cases} J^C(x,y) = \frac{I^C(x,y) - A^C}{t^C(x,y)} + A^C, \mathrm{t^C} \in (0,1] \\ I^C(x,y) = A^C, \mathrm{t^C} = 0 \end{cases} \tag{6}$$

There is no need to discuss *Cov* when $\mathrm{t^C} = 0$, because the sensor can not capture the target scene's information. When $\mathrm{t^C} \in (0,1]$,we get:

$$\mathrm{Con} = \sum_{C\in\{R,G,B\}} \sum_{(\mathrm{x,y})} \frac{\left(I^{\mathrm{C}}(x,y) - \overline{I^{\mathrm{C}}(x,y)}\right)^2}{\mathrm{N}t^{\mathrm{C}}(\mathrm{x,y})^2} \tag{7}$$

where $\overline{I^C(x,y)}$ represents the average value of C channel of the underwater image pixel acquired by the sensor; $I^C(x,y)$ represents the pixel value at (x,y) in C channel. We want the value of *Con* to be as large as possible; that is, when the acquired image $I^C(x,y)$ is determined, we want t^C to be as small as possible.

Moreover, we take $t^C(x,y)$ and A^C as constants, and the mapping of the ideal image $J^C(x,y)$ and underwater image $I^C(x,y)$ captured by the camera as shown in the figure 7 under certain conditions.

In practice, our image data type is uint8, and the range of value of $\mathrm{J^C}(\mathrm{x,y})$ and $\mathrm{I^C}(\mathrm{x,y})$ is between $[0, 255]$. If a pixel value in the image is greater than 255 in the image, the

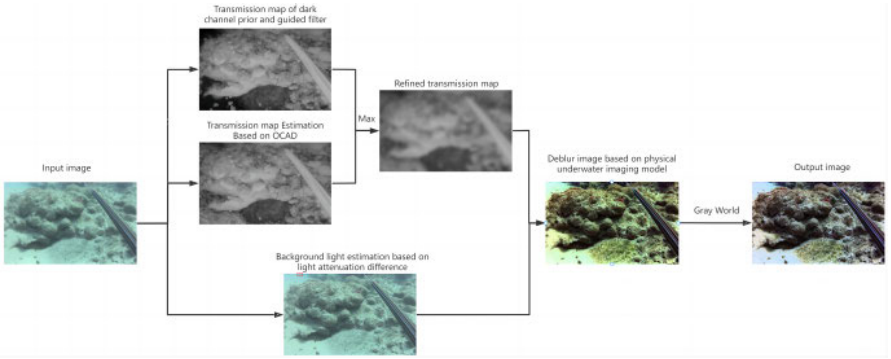

FIGURE 5. Method for enhancing underwater images based on Optimal Contrast and Attenuation Difference (OCAD).

FIGURE 6. Clear underwater image and blurred underwater image, and their *Con* value. *Con* value of left ground truth image is $1.19 * 10^4$, *Con* value of right underwater image is $1.11 * 10^4$.

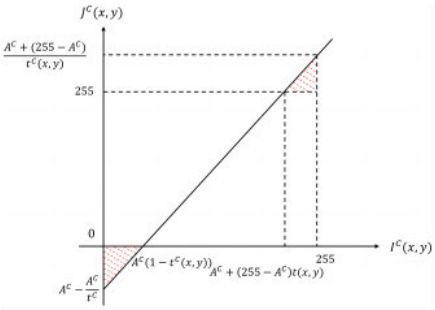

FIGURE 7. The mapping with the ideal image $J^C(x, y)$ and $I^C(x, y)$ collected by the camera.

computer thinks that the pixel value is 255. If a pixel value in the image is less than 0, the computer pretends that the pixel value is 0. The red-shaded area in figure 7 indicates that some data overflowed the range [0, 255] during the mapping from $I^C(x, y)$ to $J^C(x, y)$. The overflowing data corresponds to the black and white dots in the image corresponding to $J^C(x, y)$, meaning that this part of the data has been lost.

To effectively map more data and reduce data loss, we hope to control the value range of the ideal image to be between [0, 255].

$$0 \le J^C(x, y) \le 255 \tag{8}$$

The above expression indicates that the minimum value of the image $J^C(x, y)$ is equal to or greater than 0 and the maximum value is equal to or less than 255. So the transmission map $t^C(x, y)$follows below relationship.

$$t^C(x, y) \ge \frac{I^C(x, y) - A^C}{-A^C} \tag{9}$$

$$t^C(x, y) \ge \frac{I^C(x, y) - A^C}{255 - A^C} \tag{10}$$

$$t^C(x, y) \ge \max\left\{\frac{I^C(x, y) - A^C}{-A^C}, \frac{I^C(x, y) - A^C}{255 - A^C}\right\} \tag{11}$$

Furthermore, we want the *Con* value to be as large as possible, so $t^C(x, y)$ should be as small as possible from Equation (7), so we can get a coarse transmission map following Equation (12).

$$t^C(x, y) = \max\left\{\frac{I^C(x, y) - A^C}{-A^C}, \frac{I^C(x, y) - A^C}{255 - A^C}\right\} \tag{12}$$

Then, we get another estimate of transmission map $t_{DCP}(x, y)$ based on dark channel prior, that prior is significantly better than other algorithms in defogging, and it has a remarkable effect on removing the blur caused by scattering for the underwater image.

$$t_{DCP}(x, y) = 1 - \min_{c \in \{r,g,b\}} \left(\min_{(x,y) \in \Omega} \frac{I^c(x, y)}{A^c}\right) \tag{13}$$

When $t^C(x, y) = 1$, the light reaches the camera from the target scene and is unaffected by the attenuation effect. We can get the following Equation (14).

$$I^C(x, y) = J^C(x, y) \tag{14}$$

Equation (14) indicates that when $t^C(x, y)$ is larger and closer to 1, the acquired underwater image is closer to the target scene. So, we select the maximum value in corresponding position (x, y) of estimated transmission maps to obtain the optimal $t^C(x, y)$.

$$t^C(x, y) = \max\left\{\frac{I^C(x, y) - A}{-A}, \frac{I^C(x, y) - A}{255 - A}, t_{DCP}(x, y)\right\} \tag{15}$$

Moreover, guided filtering can optimize the halo and block shadows in the image. There is a halo and block in $t^C(x, y)$ because the dark channel prior estimates the transmission map based on the processing in image blocks.So, we use guided filter to refine $t^C(x, y)$.

B. VEILING LIGHT ESTIMATION

For Equation (2), when $r \to +\infty$, we can get the following Equation (16).

$$I^C(x_{+\infty}, y_{+\infty}) = J^C(x_{+\infty}, y_{+\infty})\, e^{-\beta^C(+\infty)} - A^C\left(1 - e^{-\beta^C(+\infty)}\right) \tag{16}$$

where $(x_{+\infty}, y_{+\infty})$ represents the point in the target scene that is an infinity away from the camera and the pixel in the underwater image. And $e^{-\beta^C(+\infty)} \to 0$, we can conclude that veiling light A^C approaches the pixel value $I^C(x_{+\infty}, y_{+\infty})$, which represents the pixel value of the farthest point from the camera to the target scene in the underwater image is the estimation of veiling light.

Most of the underwater images are blue or green hue, this is because the blue light and green light travel farther than red light in the underwater environment. The relevant information carried by the blue light of the object at the same distance in the target scene is transmitted to the camera more than the relevant information carried by the red color. So we believe that the difference between the blue or green light component and the red light component of the point farthest from the camera in the target scene is the largest, and the pixel value of this point in the underwater image is veiling light estimation.

$$(x_{\max}, y_{\max}) = \operatorname{argmax}\left(I^{G,B}(x, y) - I^R(x, y)\right) \tag{17}$$

$$A^C = I^C(x_{\max}, y_{\max}),\ C \in \{R, G, B\}) \tag{18}$$

When $(x_{\max}, y_{\max})$ corresponds to multiple points, the value of veiling light A^C is the average value of these pixels.

$$A^C = \overline{I^C(x_{\max}, y_{\max})} \tag{19}$$

The coarse enhanced underwater image $J^C(x, y)$ based on the underwater physical imaging model can be obtained by substituting $J^C(x, y)$ and A^C into Eq.2.

The veiling light is obtained by considering the differential attenuation of red, green, and blue lights. Therefore, A^C can correct the color of underwater images to a certain extent. Then we introduced the gray world theory to correct the underwater image's color to get the final enhanced underwater image.

IV. EXPERIMENT AND ANALYSIS

We select 7010 images from the Enhancing Underwater Visual Perception (EUVP) dataset and the Underwater Image Enhancement Benchmark (UIEB) dataset as our dataset. In the experimental section, we first prove that our method can remove the blur of underwater images and correct the color cast of underwater images by comparing them with Dark Channel Prior (DCP) and Gray World (GW). Then we prove that our method significantly enhances underwater images and is superior to other existing methods by comparing it with RGHS, ULAP, FUnIE, and IFM methods through quantitative and qualitative analysis.

A. DATASETS AND EVALUATION METRIC

The Enhancing Underwater Visual Perception (EUVP) [31] dataset contains separate sets of paired and unpaired image samples with poor and good perceptual quality to facilitate supervised training of models to enhance underwater images. This dataset contains 5550 dark underwater images for training the underwater image enhancement task and 570 dark underwater images for validation. We select these 6120 images for validation of our method. The UIEB (Underwater Image Enhancement Benchmark) [27] dataset includes two subsets: 890 raw underwater images with corresponding high-quality reference images and 60 challenging underwater images. We choose 890 raw underwater images for validation of our method. The EUVP and UIEB datasets provide a ground truth of low-quality underwater images. In addition, we also use the RUIE dataset [33] in the experiment. The RUIE dataset provides label files for underwater target detection but does not provide ground truth underwater images.

Then we prove that our method significantly enhances underwater images and is superior to other existing methods by comparing it with RGHS, ULAP, FUnIE, and IFM methods through quantitative and qualitative analysis. In the quantitative analysis, we mainly evaluated the image quality by using the commonly used metrics, PSNR (peak signal-to-noise ratio), SSIM (structural similarity index) [34] and UCIQE (underwater color image quality evaluation) [35], to evaluate underwater images. PSNR reflects the difference between the enhanced image and the ground truth image. SSIM comprehensively evaluates the image quality from three aspects: Illumination, Contrast, and Structure. PSNR and SSIM were calculated using reference images. We used the ideal image ground truth to calculate the index to evaluate the image quality. The higher the value of these indicators, the better the image quality. UCIQE is a linear combination of color density, saturation, and contrast used to quantitatively evaluate uneven color, blur, and low contrast of underwater images. The index does not require a reference image, and the image quality assessment result can be calculated directly from a single image. UIQM [34] evaluates underwater image quality in Lab color space without ground truth image.

B. COMPARISON WITH DARK CHANNEL PRIOR

Both DCP and OCAD can deblur underwater images. As shown in figure 8, comparing the three images in (8) is obvious. The amphiprioninae in the yellow box of the input image is blurred, while the amphiprioninae is visible in the DCP result and the result of OCAD. The result from OCAD also eliminates the blue background light from the image, making it appear brighter and clearer. In each group of images, the input images have a strong blue hue and are blurrier than those in the corresponding rows. Although the DCP result is clear, it has a strong blue hue. The details comparison in the yellow box of (6) (7) (8) in figure 8 is shown in figure 9.

In (6) (7) (8) of figure 9, the objects appear to be shrouded in fog, and the edges of the objects in the image and the

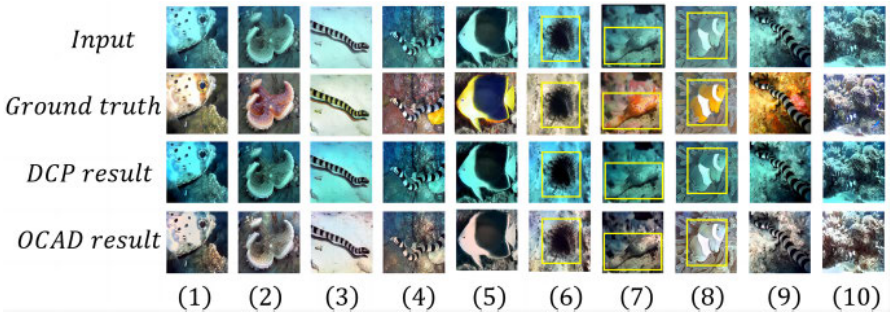

FIGURE 8. The comparison between our OCAD and DCP methods for enhancing underwater images. The first row is the original underwater image, the second row is the Ground truth provided by the EUVP dataset, the third row is the processing result of DCP, and the fourth row is the processing result of OCAD.

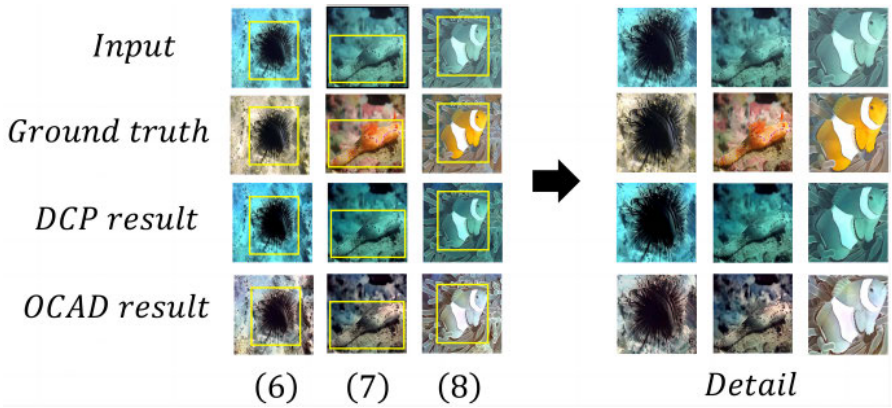

FIGURE 9. The detailed comparison in the yellow box of (6) (7) (8) in figure 8.

TABLE 1. Quantitative comparison of DCP results and OCAD results in EUVP dataset. The values in the table are the average of each image in EUVP dataset.

	DCP	OCAD
PSNR	13.90	**18.47**
SSIM	0.77	**0.86**
UIQM	0.87	**0.98**
UCIQE	0.11	**0.25**

background are the same color, so the target objects in the image are not visible. Our OCAD method removes the blur in the image and corrects the image's color so that the image looks clearer and the details of objects become more apparent. The OCAD method is more effective for other sets of images than the DCP method on underwater image deblurring and color correction tasks.

Data in bold in Table 1 are compared with the same data group, and the value is greater. The Evaluation metrics of images proposed by OCAD are better than those processed by the DCP method. OCAD is generally superior to DCP in quantitative and qualitative analysis.

C. COMPARISON WITH GRAY WORLD

As shown in figure 10, both GW and OCAD can correct the color of underwater images. In particular, the background light of the images in groups (6), (7), (9), and (10) are obviously eliminated, and the colors of the images are corrected. From the comparison of the five image groups (1), (2), (3), (5), and (8), it can be seen that OCAD corrects the color of the underwater image, making the color of the red object in each image group brighter, has an obvious deblurring ability and eliminates the fog on the GW result.

In groups (6), (7), (9), and (10), both the GW result and the result from OCAD show corrections for the green background in the input image, again proving that the OCAD method has significant color correction capabilities and both results from OCAD show blurring that cannot be removed in the GW results.

The input image in the (4) images has the better image quality and is less affected by the underwater environment. The OCAD method results show that the better-quality image has not deteriorated due to over-processing.

The detailed comparison of (2) (3) (6) of figure 10 is shown in figure 11. As you can see in detail in (2) and (3), OCAD eliminates visible fog in the input image and GW result. The coral in the yellow box is brightly colored. In (6), the result from OCAD in the yellow box shows much better color and sharpness than the input image and the GW result.

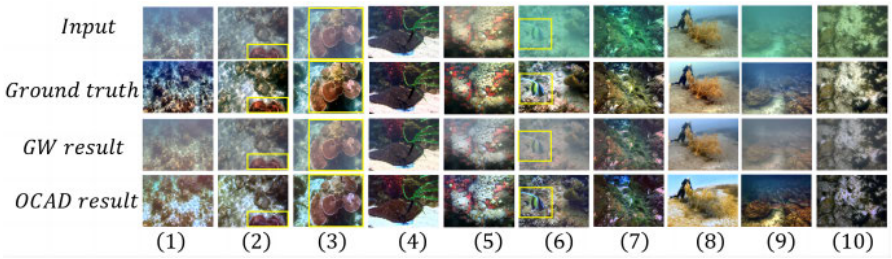

FIGURE 10. The comparison between OCAD and GW in enhancing underwater images. The first row is the original underwater image; the second is the Ground truth provided by the UIEB dataset; the third is the processing result of GW; and the fourth is the processing result of OCAD.

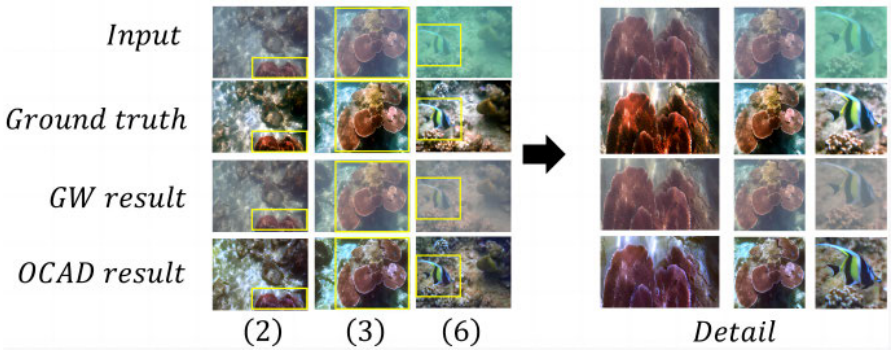

FIGURE 11. The detailed comparison of (2) (3) (6) of figure 10.

TABLE 2. Quantitative comparison of Gray World results and OCAD results in UIEB dataset. The values in the table are the average of each image in the UIEB dataset.

	GW	OCAD
PSNR	**17.01**	15.17
SSIM	**0.80**	0.79
UIQM	0.82	**0.92**
UCIQE	0.19	**0.31**

Bold data in Table 2 is more significant than the same data group; This shows that the OCAD method can improve the image's color density, saturation, and contrast better than the GW method. In general, the OCAD method is superior to the GW method in some respects.

As shown in Table 2, the images processed by our OCAD method have achieved higher scores in the metrics UIQM and UCIQE, which do not require ground truth images. In the UIEB dataset, the ground truth images are synthesized by underwater image enhancement algorithms, and these images can not fully reflect the real information of the target scene. So the comparisons of PSNR and SSIM are not convincible. In contrast, the metrics UIQM and UCIQE achieved from the enhanced image are more convincing. Moreover, the images processed by our OCAD method have obtained higher UIQM and UCIQE.

D. COMPARISON WITH OTHER METHODS

Here is a comparison of some OCAD and RGHS, ULAP, FUnIE, and IFM methods.

TABLE 3. Quantitative comparison of each method in UIEB dataset. The values in the table are the average of each image in the UIEB dataset.

	RGHS	ULAP	IFM	OCAD
PSNR	19.22	16.47	**21.94**	15.17
SSIM	0.85	0.77	**0.91**	0.79
UIQM	0.76	0.76	**0.94**	0.92
UCIOE	0.36	**0.43**	0.24	0.31

Figure 12 shows that the OCAD method can eliminate the image's blue or green background light and the fog-like blur in the image and make the scene information more in line with the actual situation. The yellow box shows that the backgrounds of (1) and (10) are more apparent. The OCAD in (2) removes the blur of the image and restores the green color attached to the stone in the background of the image well. The OCAD method in (3) eliminates the influence of the green background light on the image, (4) (5) restores the green seaweed in the image well, and the yellow box in (6) shows that the OCAD method restores the purple in the yellow box coral. (7) The details of the fishtail in the OCAD result are the clearest. (8) The green turtleback attached to the seaweed is restored. (9) The image is brighter, and there is no reddish color distortion of FUnIE. (1) and (10) The background detail inside the yellow box is clearer.

The detailed comparison of (1), (6), (7), (8), and (10) in figure 12 are shown in figure 13 and figure 14.

The bold data in Table 3 shows that the values of various metrics of images processed by OCAD are at the middle level in the UIEB dataset. Because the size of the image processed by FUnIE changes, it is inconvenient to calculate

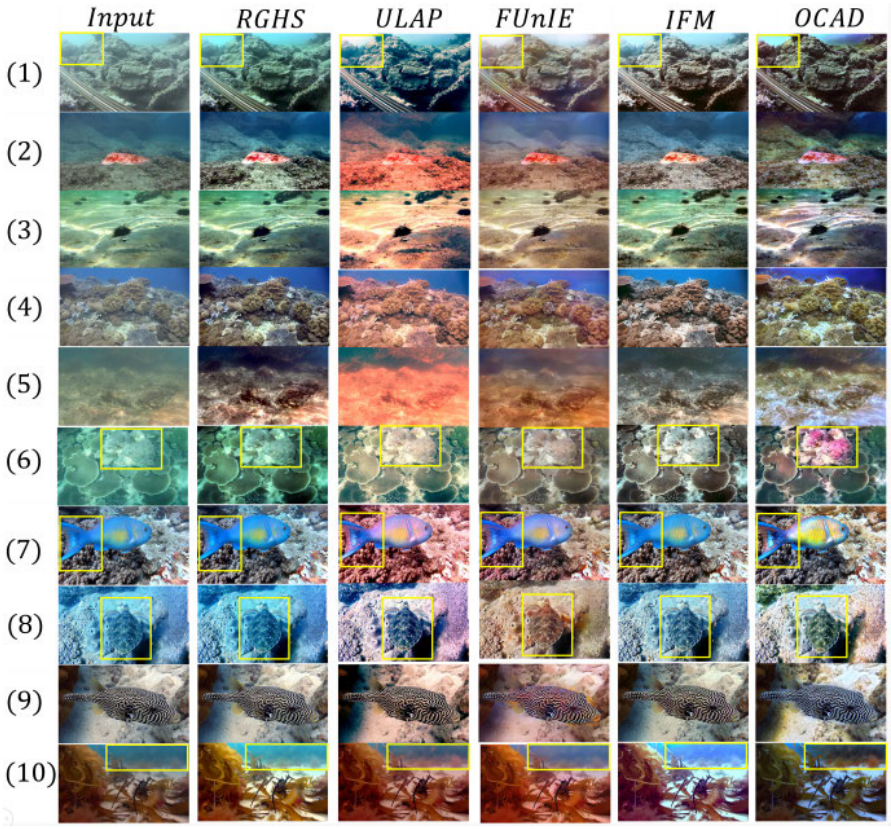

FIGURE 12. Input images and comparison of OCAD and other methods in UIEB dataset.

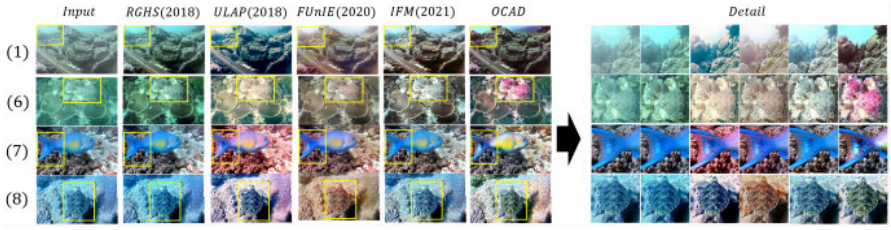

FIGURE 13. The detailed comparison of (1) (6) (7) (8) in figure 12.

FIGURE 14. The background detailed comparison of (10) in figure 12.

its image evaluation index. So, only comparing the evaluation indexes of the images processed by the other methods is calculated. In general, OCAD can realize underwater image color correction and underwater image deblurring at the same time, and the correction effect has some advantages in the UIEB dataset.

The bold data in Table 4 shows that the values of various metrics of images processed by OCAD have obvious advantages in the EUVP dataset. In general, OCAD can realize underwater image color correction and underwater image deblurring at the same time, and the correction effect has obvious advantages in the EUVP dataset.

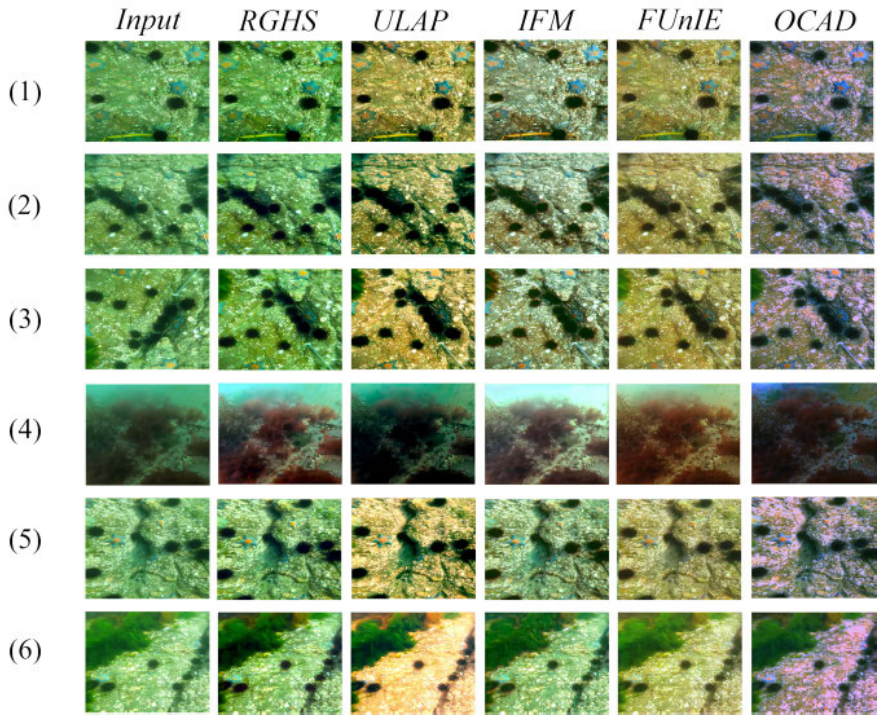

FIGURE 15. Input images and comparison of OCAD and other methods in RUIE dataset.

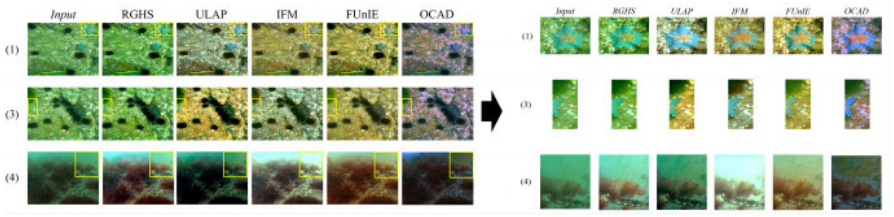

FIGURE 16. The detailed comparison of (1) (3) (4) of figure 15.

TABLE 4. Quantitative comparison of each method in the EUVP dataset. The values in the table are the average of each image in the EUVP dataset.

	RGHS	ULAP	IFM	OCAD
PSNR	15.16	17.06	16.75	**18.47**
SSIM	0.81	0.81	0.84	**0.86**
UIQM	0.97	0.97	0.97	**0.98**
UCIQE	0.35	**0.54**	0.23	0.25

As shown in figure 15 and figure 16, images processed by OCAD has obvious deblurring and color correction effect compared with original underwater images and images processed by other methods, and the background information of the image is better preserved, as shown in (4) of Figure16.

RUIE dataset does not provide ground truth images, so we only compare UCIQE and UIQM of images processed by each method. The bold data in Table 5 shows that the values of various metrics of images processed by OCAD are at the middle level. The performance of the OCAD method on the RUIE dataset has a certain corrective effect.

TABLE 5. Quantitative comparison of each method in RUIE dataset. The values in the table are the average of each image in RUIE dataset.

	RGHS	ULAP	IFM	OCAD
UIQM	**0.73**	0.19	0.70	0.33
UCIQE	0.26	**0.28**	0.18	0.23

As shown in Table 3, Table 4, and Table 5, our OCAD algorithm performs better on the EUVP dataset. Moreover, the images in the EUVP dataset have a heavy blue or green tone; these images are collected close-up in a deepsea environment. The G channel and B channel contain much more practical information about the target scene than the R channel in the deep-sea environment, which is very consistent with the basic idea of attenuation difference in our OCAD method, so our OCAD method is suitable for this kind of scene. The images processed by OCAD can better reflect the factual information of objects in the deep-sea environment. The metrics comparison of our OCAD method obtained higher PSNR, SSIM, and UIQM values, as shown in Table 4, so the OCAD method has obvious advantages in the EUVP dataset.

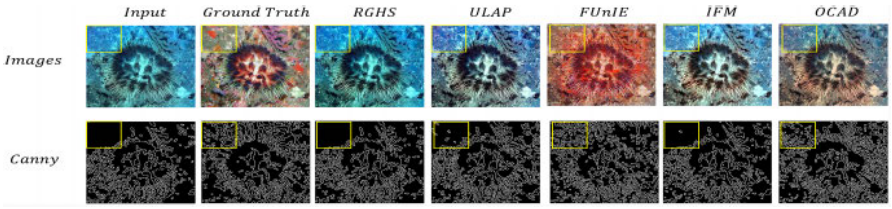

FIGURE 17. Canny results comparison of each method mentioned in Subsection D. The first row is the original image, ground truth image, and the results of each method, and the second row is Canny results of these images.

The comparison in Table 3 and Table 5 also shows that our OCAD method lacks ability when dealing with the colorful UIEB dataset. However, the images processed by our OCAD method have obvious deblurring and color correction results; the UIQM and UCIQE metrics values are not the highest. Our OCAD method is generally suitable for the EUVP dataset, which is suitable for deep-sea close-range images; the experiments show that our OCAD method achieved significant image enhancement. However, there is still room to improve. We will combine deep learning methods in future research to improve the robustness and generalization of our OCAD method.

E. COMPARISON OF DETAIL EXTRACTION

We compare the Canny results of the enhanced underwater images by the methods mentioned in Subsection D. We normalize the images and use the Canny method to extract the images' edges.

As shown in figure 17, the FUnIE result has obvious noises, so its corresponding Canny result has the most white lines, even more than the Canny result of ground truth. The stones in the yellow box have obvious texture features. Except for the Canny result corresponding to FUnIE, which introduces a lot of noise, other methods lose the texture features of the stone in the background of the image.

Overall, our OCAD method can significantly improve the underwater image quality and restore the background features of the degraded underwater image.

V. CONCLUSION

We proposed an OCAD method and demonstrated the significant advantages of this method over other methods, both qualitatively and quantitatively.

We compared the EUVP and UIEB underwater image data sets with the state-of-the-art and classical underwater image enhancement algorithms and analyzed them in detail. The experimental results show that our algorithm can enhance underwater images significantly and is superior to other methods. We have experimentally verified that the OCAD method has significant underwater image enhancement capability.

Although the OCAD method achieves good qualitative and quantitative evaluation results in most cases, it may distort the results when processing images with an extensive background but no major object. In future research, we plan to semantically divide the image into background and object parts by segmenting the object into specular and diffuse reflective objects for future processing. We believe more targeted and selective image processing will lead to better processing results.

REFERENCES

[1] G. Bailey and N. Flemming, "Archaeology of the continental shelf: Marine resources, submerged landscapes and underwater archaeology," *Quaternary Sci. Rev.*, vol. 27, nos. 23–24, pp. 2153–2165, Nov. 2008.

[2] S. Q. Duntley, "Light in the sea," *J. Opt. Soc. Amer.*, vol. 53, no. 2, pp. 214–233, 1963.

[3] Y. Y. Schechner and Y. Averbuch, "Regularized image recovery in scattering media," *J. IEEE Trans. Pattern Anal. Mach. Intell.*, vol. 29, no. 9, pp. 1655–1660, Sep. 2007.

[4] X. Shao, F. Liu, W. Li, L. Yang, S. Yang, and J. Liu, "Latest progress in computational imaging technology and application," *J. Laser Optoelectron. Prog.*, vol. 57, no. 2, Feb. 2020, Art. no. 020001.

[5] J. S. Jaffe, "Computer modeling and the design of optimal underwater imaging systems," *IEEE J. Ocean. Eng.*, vol. 15, no. 2, pp. 101–111, Apr. 1990.

[6] J. Watson, "Underwater visual inspection and measurement using optical holography," *Opt. Lasers Eng.*, vol. 16, nos. 4–5, pp. 375–390, Jan. 1992.

[7] Z. Xin-Wei, J. Tao, C. Hao, and Q. Song, "Modeling and simulation of the background light in underwater imaging under different illumination conditions," *Acta Phys. Sinica*, vol. 64, no. 10, 2015, Art. no. 104201.

[8] D. Akkaynak, T. Treibitz, T. Shlesinger, Y. Loya, R. Tamir, and D. Iluz, "What is the space of attenuation coefficients in underwater computer vision?" in *Proc. IEEE Conf. Comput. Vis. Pattern Recognit. (CVPR)*, Honolulu, HI, USA, Jul. 2017, pp. 568–577.

[9] D. Akkaynak and T. Treibitz, "A revised underwater image formation model," in *Proc. IEEE/CVF Conf. Comput. Vis. Pattern Recognit.*, Salt Lake City, UT, USA, Jun. 2018, pp. 6723–6732.

[10] D. Akkaynak and T. Treibitz, "Sea-thru: A method for removing water from underwater images," in *Proc. IEEE/CVF Conf. Comput. Vis. Pattern Recognit. (CVPR)*, Long Beach, CA, USA, Jun. 2019, pp. 1682–1691.

[11] P. Han, F. Liu, Y. Wei, and X. Shao, "Optical correlation assists to enhance underwater polarization imaging performance," *Opt. Lasers Eng.*, vol. 134, Nov. 2020, Art. no. 106256.

[12] F. Feng, G. Wu, Y. Wu, Y. Miao, and B. Liu, "Algorithm for underwater polarization imaging based on global estimation," *J. Acta Opt. Sin.*, vol. 40, no. 21, pp. 75–83, Nov. 2020.

[13] G. Jin-ge, Z. Yong, Z. Yong-qiu, M. Miao, S. Peng, and X. Chen-yang, "Optical polarization imaging for underwater target detection with non-scatter background," *J. Meas. Sci. Instrum.*, vol. 11, no. 4, pp. 335–342, Dec. 2020.

[14] R. Hummel, "Image enhancement by histogram transformation," *J. Comput. Graph. Image Process.*, vol. 6, no. 2, pp. 184–195, Apr. 1977.

[15] Y. Y. Schechner and N. Karpel, "Recovery of underwater visibility and structure by polarization analysis," *IEEE J. Ocean. Eng.*, vol. 30, no. 3, pp. 570–587, Jul. 2005.

[16] K. Herkül, A. Peterson, and S. Paekivi, "Applying multibeam sonar and mathematical modeling for mapping seabed substrate and biota of offshore shallows," *J. Estuarine, Coastal Shelf Sci.*, vol. 192, pp. 57–71, Jun. 2017.

[17] T. Yang, S. Jia, and H. Ma, "Research on the application of super resolution reconstruction algorithm for underwater image," *J. Comput., Mater. Continua*, vol. 62, no. 3, pp. 1249–1258, 2020.
[18] R. Fattal, "Single image dehazing," *J. ACM Trans. Graph.*, vol. 27, no. 3, pp. 1–9, 2008.
[19] N. Carlevaris-Bianco, A. Mohan, and R. M. Eustice, "Initial results in underwater single image dehazing," in *Proc. OCEANS MTS/IEEE SEATTLE*, Seattle, WA, USA, Sep. 2010, pp. 1–8.
[20] K. He, J. Sun, and X. Tang, "Single image haze removal using dark channel prior," in *Proc. IEEE Conf. Comput. Vis. Pattern Recognit.*, Miami, FL, USA, Jun. 2009, pp. 1956–1963.
[21] K. He, J. Sun, and X. Tang, "Guided image filtering," *IEEE Trans. Pattern Anal. Mach. Intell.*, vol. 35, no. 6, pp. 1397–1409, Jun. 2013.
[22] M. Han, Z. Lyu, T. Qiu, and M. Xu, "A review on intelligence dehazing and color restoration for underwater images," *J. IEEE Trans. Syst., Man, Cybern. Syst.*, vol. 50, no. 5, pp. 1820–1832, May 2020.
[23] D. Huang, Y. Wang, W. Song, J. Sequeira, and S. Mavromatis, "Shallow-water image enhancement using relative global histogram stretching based on adaptive parameter acquisition," in *Proc. Int. Conf. Multimedia Model.*, Bangkok, Thailand, Feb. 2018, pp. 453–465.
[24] H. Hu, Y. Zhang, X. Li, Y. Lin, Z. Cheng, and T. Liu, "Polarimetric underwater image recovery via deep learning," *J. Opt. Lasers Eng.*, vol. 133, Oct. 2020, Art. no. 106152.
[25] W. Song, Y. Wang, D. Huang, and D. Tjondronegoro, "A rapid scene depth estimation model based on underwater light attenuation prior for underwater image restoration," in *Advances in Multimedia Information Processing—PCM*. Hefei, China: Springer, Sep. 2018.
[26] D. Berman, D. Levy, S. Avidan, and T. Treibitz, "Underwater single image color restoration using haze-lines and a new quantitative dataset," *J. IEEE Trans. Pattern Anal. Mach. Intell.*, vol. 43, no. 8, pp. 2822–2837, Aug. 2021.
[27] C. Li, C. Guo, W. Ren, R. Cong, J. Hou, S. Kwong, and D. Tao, "An underwater image enhancement benchmark dataset and beyond," *J. IEEE Trans. Image Process.*, vol. 29, pp. 4376–4389, 2020.
[28] R. Liu, Z. Jiang, S. Yang, and X. Fan, "Twin adversarial contrastive learning for underwater image enhancement and beyond," *J. IEEE Trans. Image Process.*, vol. 31, pp. 4922–4936, 2022.
[29] Z. Ma and C. Oh, "A wavelet-based dual-stream network for underwater image enhancement," in *Proc. IEEE Int. Conf. Acoust., Speech Signal Process. (ICASSP)*, Singapore, Singapore, May 2022, pp. 2769–2773.
[30] Y. Lai, Z. Zhou, B. Su, Z. Xuanyuan, J. Tang, J. Yan, W. Liang, and J. Chen, "Single underwater image enhancement based on differential attenuation compensation," *J. Front. Mar. Sci.*, vol. 9, Nov. 2022, Art. no. 1047053.
[31] M. J. Islam, Y. Xia, and J. Sattar, "Fast underwater image enhancement for improved visual perception," *J. IEEE Robot. Autom. Lett.*, vol. 5, no. 2, pp. 3227–3234, Apr. 2020.
[32] X. Chen, P. Zhang, L. Quan, C. Yi, and C. Lu, "Underwater image enhancement based on deep learning and image formation model," 2021, *arXiv:2101.00991*.
[33] R. Liu, X. Fan, M. Zhu, M. Hou, and Z. Luo, "Real-world underwater enhancement: Challenges, benchmarks, and solutions under natural light," *J. IEEE Trans. Circuits Syst. Video Technol.*, vol. 30, no. 12, pp. 4861–4875, Dec. 2020.
[34] K. Panetta, C. Gao, and S. Agaian, "Human-visual-system-inspired underwater image quality measures," *IEEE J. Ocean. Eng.*, vol. 41, no. 3, pp. 541–551, Jul. 2016.
[35] M. Yang and A. Sowmya, "An underwater color image quality evaluation metric," *J. IEEE Trans. Image Process.*, vol. 24, no. 12, pp. 6062–6071, Dec. 2015.

TENGHUI WANG received the B.S. degree in electronic information engineering from Xinyang Normal University, Henan, China, in 2019, and the M.S. degree in data science from the City University of Macau, Macao, China, in 2021. He is currently pursuing the Ph.D. degree in computer application technology with Macao Polytechnic University, Macau. He is also a Lecturer with the Smart Vision Research and Innovation Center, Faculty of Information Technology, Beijing Institute of Technology, Zhuhai. His research interests include computer vision, digital image processing, and artificial intelligence.

LILI WANG received the M.S. degree in public administration from the Beijing Institute of Technology, Beijing, China, in 2011. She is currently an Assistant Researcher with the Beijing Institute of Technology, Zhuhai, and the Assistant Dean of the Faculty of Information Technology. Her research interests include underwater image enhancement, project management, and public administration.

EN ZHANG received the M.S. degree in control and cybernetics from the Beijing Institute of Technology, Beijing, China, in 2005. He is currently pursuing the Ph.D. degree in data science with the City University of Macau. He is currently a Lecturer with the Beijing Institute of Technology, Zhuhai. His research interests include control theory and methods, fault diagnosis, machine learning, and predictive maintenance.

YAN MA received the Graduate degree from the Beijing University of Posts and Telecommunications (BUPT), Beijing, China. He is currently a Professor with the Computer Science Department, BUPT. He has been teaching and doing research in the field of computer network and telecommunications. He has received several National Science and Technology Awards.

YAPENG WANG (Member, IEEE) received the B.Sc. degree from North China Electric Power University, China, in 1998, and the M.Sc. and Ph.D. degrees from the Queen Mary University of London, U.K., in 2002 and 2007, respectively. He joined the Faculty of Applied Sciences, Macao Polytechnic University, in 2021, as an Associate Professor. His current research interests include applied artificial intelligence, wireless communications, automatic speech recognition, and machine learning.

HAIJUN XIE received the B.S. degree in mechanical design manufacture and automation from Huazhong Agricultural University, Hubei, China, in 2003, and the M.S. and Ph.D. degrees in agricultural mechanization engineering from South China Agricultural University, Guangzhou, China, in 2006 and 2017, respectively. He is currently an Associate Professor with the Beijing Institute of Technology, Zhuhai. His research interests include smart agriculture, intelligent manufacturing, and intelligent machining.

MINGCHAO ZHU received the B.S. degree in electronic science and technology from the Beijing Institute of Technology, Zhuhai, China, in 2010, and the M.A. degree (Hons.) in communication with a concentration in artificial intelligence and digital media from Baptist University, Hongkong, China, in 2021. He is currently pursuing the Ph.D. degree in data science with the City University of Macau, Macau, China. He is also a Lecturer with courses mainly, including Python Programming and Java Programming with the Faculty of Information Technology, Beijing Institute of Technology, Zhuhai. His research interests include artificial intelligence, computer vision, and pattern recognition.